International Journal of Biological Macromolecules 247 (2023) 125795

Contents lists available at ScienceDirect

International Journal of Biological Macromolecules

journal homepage: www.elsevier.com/locate/ijbiomac

Chachafruto starch: Physicochemical characterization, film-forming properties, and 3D printability

Luis Daniel Daza [a,b,*], Miguel Ángel Montealegre [b], Cristina Reche [a], Angélica Sandoval-Aldana [b], Valeria Soledad Eim [a,*], Henry Alexander Váquiro [b]

[a] Department of Chemistry, University of the Balearic Islands, Ctra. Valldemossa km. 7.5, 07122 Palma de Mallorca, Spain
[b] Departamento de Producción y Sanidad Vegetal, Facultad Ingeniería Agronómica, Universidad del Tolima, 730006 Ibagué, Colombia

ARTICLE INFO

Keywords:
Erythrina edulis Triana
Food packaging
Edible inks

ABSTRACT

This work aimed to characterize the physicochemical, film-forming properties, and 3D printability of a nonconventional starch from chachafruto. The chachafruto native starch (CHS) presented an excellent extraction yield (10 % db) and purity (99 % db), along with an oval and round morphology, a smooth surface with few defects, and a mean diameter of 15.4 μm. The typical B-type diffraction pattern was observed in the CHS with a crystallinity of 17.4 %. The starch presented a paste temperature of 66.1 °C, an enthalpy of 11.5 J g^{-1}, and a final viscosity of 596 Brabender Units. The thermal analysis demonstrated good thermal stability. The evaluated film presented a reduction in crystallinity (8.18 %) to the CHS, which generated a good elasticity in the material. Likewise, it presented a continuous structure without cracks, providing good barrier properties (2.3 × 10^{-9} g•m^{-1}•s^{-1}•Pa^{-1}) and high transparency. Meanwhile, 3D prints prepared with CHS showed good textural properties and high consistency. The morphological analysis showed that the prints generated organized cell structures. However, high concentrations of CHS were not efficient in obtaining 3D prints. The results of this work demonstrate the tremendous industrial potential of chachafruto as an unconventional source of starch and some alternative uses for adding value to the crop.

1. Introduction

Starch is a natural polysaccharide in cereal grains, legumes, tuber, and root crops. This macromolecule is consumed worldwide and is used as a raw material in different industries such as pharmaceuticals, food, biomedical, and plastics [1]. By 2026, the production of this material is expected to reach 120 million tons, with corn, wheat, cassava, and potatoes being its primary sources [2]. This situation has generated concern worldwide about the possible impact on food security, which has led to the search for alternative sources of starch in its native form [3–5]. However, the chemical composition of the starches obtained from these alternative sources, as well as their industrial potential, may vary according to the crop's botanical source and agro-ecological conditions. Consequently, it is necessary to characterize the physicochemical properties and evaluate their industrial potential.

The chachafruto (*Erythrina edulis* Triana) is a legume plant native to South America, cultivated mainly at altitudes between 1600 and 2000 m above sea level. The plant has a broad spectrum of uses ranging from animal feed (as fodder) to soil recovery due to its nitrogen fixation capacity in soils [6]. The seeds have a high protein content with values ranging from 18 % to 24 %, as well as a high content of carbohydrates (70 %), mainly starch (28.6 % db) [7–9]. Despite its nutritional potential, its use in the human diet is limited and is restricted to consumption by local populations. The lack of a chachafruto industry represents an opportunity for exploitation and adding value to this crop. Recent studies have focused on obtaining chachafruto protein fractions with different biological potentials [7,10]. However, the studies focused on revaluing the starch obtained from its seeds, and its use is limited. In order to promote the integral use and exploitation of the chachafruto, as well as generating a circular economy around this crop, it is necessary to carry out studies focused on the complete characterization of the macromolecules obtained from the starch and its potential use at industrial level.

Among the alternative uses of starch in the food industry, the production of biodegradable films that can partially replace petroleum-derived plastics, has been a topic of interest and development in

* Corresponding authors at: Department of Chemistry, University of the Balearic Islands, Ctra. Valldemossa km. 7.5, 07122 Palma de Mallorca, Spain.
E-mail addresses: danieldaza08@gmail.com, l.daza@uib.es (L.D. Daza), valeria.eim@uib.es (V.S. Eim), havaquiro@ut.edu.co (H.A. Váquiro).

https://doi.org/10.1016/j.ijbiomac.2023.125795
Received 17 April 2023; Received in revised form 26 June 2023; Accepted 10 July 2023
Available online 11 July 2023

recent years largely due to its environmental impact. Different starch sources have been evaluated for preparing these biomaterials, such as sweet potato, rice, pumpkin, lentil, and quinoa starches, showing great potential for the packaging industry mainly due to their low oxygen permeability, flexibility, and optical properties [11–13]. However, the material's performance depends on the processing conditions and the starch's physicochemical properties. The characteristics of starch-based films rely on the ratio of amylose and amylopectin in the starch. Basiak et al. [14] compared biodegradable films made from wheat (25 % amylose), corn (27 % amylose), and potato (20 % amylose) starches and found differences in their barrier, mechanical and hydration properties. They reported that films with lower amylose content had lower water permeability, solubility, and better mechanical properties.

3D printing is an innovative technology that can produce food products with defined shapes by depositing one or more materials layer by layer [15,16]. This technology offers several benefits for food production, such as diet customization, process automation, time and waste reduction, as well as enhanced sensory attributes [17]. The materials used for printing must be malleable, self-supporting, quickly solidifying, and have a certain flowability that allows them to pass through the nozzle, which means that only some food materials can be used for this purpose [18]. Starch is a material that meets all these characteristics due to its ability to gelatinize and form viscoelastic gels. However, the printability properties depend on the type and properties of the starch used [17]. Zheng et al. [19] compared the effects of amylose content on 3D printing using potato, wheat, and corn starches. They found that the microstructure and texture of the 3D prints varied significantly, even with the same starch concentration (25 % *w/v*). Furthermore, printability was associated with the lowest final viscosity observed in wheat starch preparations. Starch concentration in 3D printing preparation influenced the technological properties of the materials. Qiu et al. [20] reported that higher starch concentration in gels increased the gel viscosity and the interaction of the amylose and amylopectin chains, resulting in more defective and less printable materials. Similar observations were reported for 3D prints prepared with potato starch [21]. The authors found that intermediate starch concentrations enhanced printability and the resistance of the monolayer of the 3D prints.

Considering the growing demand for new starch sources and the unexplored industrial potential of chachafruto starch, this study aimed as well, to evaluate the physicochemical characteristics and the technological potential of starch obtained from chachafruto as a novel material for edible films production and food 3D printing. The study hopes to contribute to the generation of a circular economy for the cultivation of chachafruto, as well as being the basis for added value on an industrial scale, of the starch obtained from this material.

2. Materials and methods

2.1. Materials

Chachafruto (*Erythrina edulis* Triana) was harvested on the farm "El Mirador" located in the village "La India", Coello Cocora, Ibagué city (4°22′14.2"N 75°19′16.4" W). Samples were selected and washed, and those exhibiting mechanical damage were discarded.

2.2. Starch isolation

The chachafruto samples were selected, discarding any that showed mechanical damage, washed with tap water and peeled manually. They were then cut into thin slices (approx. 2 mm) and milled using a food blender (BRLY07 – Zoo, Oster, Colombia) for 1 min with distilled water at a ratio of 1:2. The resulting mixture was filtered using a cloth sieve. Then, the solid was re-extracted, and the filtrates pooled and stored at 4 °C and left to stand for 18 h until phase separation. After this, the supernatant was discarded, and water was added to re-suspend the sediment. The mixture was filtered again using a cloth filter. This procedure was repeated four more times until a translucent supernatant was obtained. The last two washes were performed using distilled water. The chachafruto starch (CHS) obtained was dried in a forced convection oven (Thermolab, DiEs, Colombia) at 40 °C and stored at room temperature (~25 °C) in a vertical desiccator cabinet.

2.3. Chemical composition, apparent amylose content, color, and morphological characterization of chachafruto starch

The moisture (Method 925.10), protein (Method 920.87), lipids (Method 920.85), and ash (Method 923.03) contents were determined according to the methods of the A.O.A.C [22]. The total carbohydrate content was obtained by subtracting the sum of the protein, lipid, moisture, and ash content from 100. Apparent amylose content analysis was carried out according to the method reported by Galindez et al. [23]. The color parameters were obtained according to the CIELAB color system using a Konica Minolta colorimeter (Cr 410, Minolta Co., Japan). Morphological characterizations were examined with and without polarized light in optical microscopy (BX60, Olympos, Japan) coupled with a camera Moticam 3.0 MP Color Digital Camera (3.0MP, Motic, Hong Kong), as well as with scanning electron microscopy (SEM/S-3400 N, Hitachi, Germany) as reported previously by Daza et al. [1].

2.4. Particle size distribution

The particle size distribution of the CHS was evaluated using a Laser Particle Analyzer (Sync Microtrac MRB, wet operation Flowsync, Montgomeryville, PA, USA) according to Lin et al. [24]. For this purpose, the CHS was suspended in distilled water and stirred at 2000 rpm. For the analysis, water and starch refractive indexes were adjusted to 1.33 and 1.53, respectively. The samples were sonicated in the equipment at 25 Hz for 15 s before analysis, to avoid aggregation of the granules. Results were reported as diameters at 10th percentile [$d_{(0.1)}$], median [$d_{(0.5)}$], and 90th percentile [$d_{(0.9)}$].

2.5. Pasting properties, gel texture, and paste clarity

The pasting properties of CHS were evaluated using a Visco-Amylo-Graph (Micro Visco-Amylo-Graph®, Brabender Instrument Inc., Germany) according to [3]. Pasting temperature (PT), peak viscosity (PV), trough viscosity (TV), breakdown (BD), setback (SB), and final viscosity (FV) were calculated. Viscosity was expressed in Brabender Units (BU). The gels' texture was measured according to the method described by [3] using a texture analyzer with a load cell of 20 N (LS1, Lloyd Ltd., USA). The CHS gels obtained in pasting properties analysis were transferred to plastic containers (25 mm diameter, 50 mm height) and stored at 4 °C for 24 h before analysis. For the analysis, the sample gels were subjected to two compression cycles at a distance of 10 mm (0.05 N trigger force) at a speed of 0.5 mm s^{-1} by a flat-ended using a cylindrical probe (6 mm diameter). Hardness, adhesiveness, and cohesiveness were determined using Nexygen Plus software (Lloyd Ltd., Version 3.0) [25].

2.6. X-ray diffraction (XRD)

The X-ray diffraction patterns of the samples were obtained using a Bruker D8 ADVANCE diffractometer (Bruker, Billerica, USA) with Ni-filtered Cu-Kα1 radiation (40 kV and 40 mA) and a specific wavelength of 1.5406 Å. Data was collected in the 2θ range of 3.5–70° (0.02035° of step size) and a counting time of 0.8 s/ step. Relative crystallinity was calculated using the DIFFRAC.EVA software (Bruker, Billerica, USA).

2.7. Fourier-transform infrared (FTIR) spectroscopy

The FTIR spectra of the CHS were obtained using a Fourier – transform infrared spectroscopy (Nicolet 380, Thermo Scientific Inc., USA).

The measurements were recorded over the 4000 to 500 cm^{-1}, with a resolution of 4 cm^{-1} and 40 scans at room temperature (~20.4 °C).

2.8. Thermal properties

The Onset (T_0), peak (T_p), and conclusion (T_c) temperatures and enthalpy of gelatinization (ΔH) of the CHS were measured using a differential scanning calorimeter (2920, TA Instruments, Japan) according to the methodology described by Lin et al. [3]. The obtained thermograms were examined using Universal Analysis 2000 V3.9A software (TA Instruments, Japan).

CHS's thermal degradation temperature and weight loss (WL) were measured using a thermogravimetric analyzer (SDT 2960, TA instruments, Japan) over the temperature range of 20–600 °C at a heating rate of 20 °C min^{-1} and under a stream of nitrogen.

2.9. Potential as food packaging of CHS

2.9.1. The CHS – based films preparation

The CHS was dissolved in distilled water at a concentration of 2.0 % (*w/v*, dry basis d.b.) (CHSF) (this concentration was selected after preliminary analysis, data not shown) and agitated for 10 min using a magnetic agitator. The mixture was heated to 95 °C and maintained at this temperature for 5 min. Then, glycerol (1.0 % *w/v*) was added to the mixture when it reached 50 °C. The prepared solutions were cast in a Petri dish (~0.53 g of the film solution per cm^2). The films were dried at 40 °C for 24 h in a forced convection oven. Before the analyses, the samples were stabilized in a vertical desiccator cabinet at room temperature (~23 °C) and relative humidity (RH) of 54 % for 24 h.

2.9.2. CHS – based films characterization

The CHS – based films were characterized with regard to swelling power (*SP*; %), solubility (*S*, %), opacity (*OP*), mechanical properties [Young Modulus (*YM*; MPa), elongation at break (*EB*; %), tensile strength (*TS*; MPa)], morphology and water vapor permeability (*WVP*) according to the methodologies described previously by Homez-Jara et al. [26]. The XRD, FTIR, and TGA were carried out according to the methods described in previous sections.

2.10. CHS potential for 3D printing

2.10.1. Sample preparation and 3D printing

For the preparation of the starch gels, the CHS was mixed with distilled water at three concentrations [8 % (CHS3D1), 10 % (CHS3D2), and 12 % (CHS3D3) *w/v* d.b.] (selected from preliminary analysis). Then, the mixture was heated to 90 ± 2 °C with constant stirring using a mechanical stirrer (RZR 2021, Heidolph, Germany) at 180 rpm for 10 min. Then, the samples were left to stand until they reached a temperature of 60 °C and then transferred to a print cartridge (nozzle of 1.5 mm). The 3D printing was carried out in an extrusion-based 3D printer (Foodini™, Natural Machines, Spain) based on preliminary analysis and the manufacturer's specifications [27]. A cuboid model (geometry given by the machine by default) with dimensions of 20 mm × 20 mm × 10 mm was printed with a monolayer height and nozzle movement speed of 1.4 mm and 500 mm/min. Printed specimens with dimensions of 10 mm × 10 mm × 5 mm were used for the dynamic-mechanical analysis (DMA).

2.10.2. Characterization of 3D prints

The microstructural characteristics of the samples were analyzed using scanning electron microscopy (SEM/S-3400 N, Hitachi, Germany) in freeze-dried and cold-broken samples using liquid nitrogen [1,28]. Textural analysis was performed using a universal test machine (Zwick/Z100, Zwick Roell, Germany). For this purpose, each printed sample was placed in the center of a steel plate and submitted to compression (40 % of the total sample height) using a cylindrical probe at a 6 mm/min compression rate with an initial gap separation of 13 mm. The XRD parameters were adjusted according to the methodology described in the previous section (Section 2.6). Before the analysis, the samples were dried by lyophilization and ground using an analytical grinder universal mill (Yellowline A10, IKA, Germany), according to Liu et al. [29]. The DMA was evaluated according to Yang et al. [30] using a dynamic mechanical analyzer (DMA, Q800, TA Instruments, USA) with a parallel-plate geometry (diameter of 20 mm and a gap of 10 mm). The specimens (10 mm × 10 mm × 5 mm) were loaded and submitted to a compression test in a "frequency sweep" mode ranging from 0.1 to 30 Hz at a fixed strain amplitude of 1 ± 0.004 % of the total sample height and at room temperature (24 ± 2 °C). The storage modulus (G') and loss modulus (G'') of the materials were plotted and analyzed using Universal Analysis 2000 V3.9A software (TA Instruments, Japan).

2.11. Statistical analysis

The results were reported as the mean and standard deviation of each property based on at least three replicates for each sample. Analysis of variance (ANOVA) and Tukey–Kramer range tests at a significance level of 0.05 were performed to compare the properties of the biodegradable films.

3. Results and discussion

3.1. Chemical composition, apparent amylose content, color, and morphological characterization

The yield and chemical composition of the chachafruto starch (CHS) is shown in Table 1. The yield of starch obtained from chachafruto was slightly lower than the 13 % reported for the same species [31], which could be related to differences in the extraction method and agro-ecological conditions. The CHS showed acceptable moisture content considering that the maximum value for industrial use is 20 % [32]. The low content of protein, fat, lipids, and ashes in the material analyzed (< 1.0 % of the total composition) is related to the efficiency of the extraction process and the purity of the material extracted [33]. Similar

Table 1
Chemical composition, color characteristics, and particle size of chachafruto starch.

Parameter	Value ± SD
Chemical composition	
Moisture (%)	8.70 ± 0.08
Yield (% db)	9.54 ± 0.71
Protein (% db)	0.88 ± 0.17
Lipids (% db)	0.01 ± 0.00
Carbohydrates (% db)	99.1 ± 0.1
Ash (% db)	0.03 ± 0.00
Amylose (% db)	36.6 ± 1.2
Color characteristics	
L^*	98.0 ± 0.6
a^*	5.91 ± 0.04
b^*	−3.57 ± 0.08
WI	92.8 ± 0.1
Particle size distribution	
$d_{(0.1)}$ (μm)	9.0 ± 0.6
$d_{(0.5)}$ (μm)	15.4 ± 0.5
$d_{(0.9)}$ (μm)	21.9 ± 0.7
D [3, 4] (μm)	15.3 ± 0.5
D [2, 3] (μm)	10.8 ± 0.2

db: dry basis; a^*: CIELab coordinates (redness/greenness); b^*: CIELab coordinates (yellowness/blueness); L^*: CIELab coordinates (Luminosity); WI: white index; d: diameter at different percentiles. Values are expressed as means ± standard deviation of at least three repetitions.

purity results were observed in the extraction of other starches [5]. The apparent amylose content of CHS was in agreement with that of the mung bean [5] and the common bean [34]; however, it was greater than tamarind and moth bean starches [4,35]. Amylose content can influence the film-forming properties and printability of starches. Thus, starches with a high content of this molecule can produce films with more homogeneous morphologies and greater tensile strength, this being related to the organization of the network due to the retrogradation of amylose [34]. Similar to the chemical composition, the color parameters can also be associated with the purity of the extracted starch. According to Boudries et al. [28], high luminosity ($L^* > 90$) and high white index (WI) values (WI > 90) correspond to starches with high purity. In addition, the low values in parameters a^* and b^* are associated with the absence of pigments (Table 1), which can interfere with the CHS's coloration and the consumer's final perception.

The CHS granules exhibited mainly elongated and spherical shapes with smooth surfaces (Fig. 1 A-C). However, some irregular granules were observed, which may be due to a physical influence of the extraction method on some of the analyzed granules (red arrows in Fig. 1B). The morphology of the CHS is in agreement with the morphology of the bean [34], tamarind kernel [4], moth bean [35], and kidney bean [37] starches. In addition, the birefringence of the granules was confirmed with the Maltese cross observation using polarized light microscopy (Fig. 1C). The presence of the Maltese cross can be related to the integrity of the granules [38].

3.2. Particle size distribution

The starch granules obtained from the chachafruto showed a bimodal distribution (Fig. 2A). The first granule size population, corresponding to 6.78 % of the granule population and ranged between 1 and 4 μm with a mean diameter of 2.33 ± 0.31 μm (Fig. 2A). Meanwhile, the second and the main population corresponded to 93.2 % of the granule population and ranged between 6 and 44 μm with a mean diameter of 15.8 ± 0.5 μm. The bimodal distribution has also been observed in starches obtained from legumes such as mung bean [39] and kidney bean [40]. In addition, the mean granule diameter obtained for the analyzed starch (Table 1) is in accordance with the results reported for Yard-long bean seed starch [41]. However, the values obtained for CHS were lower than those observed in starches from different bean starches [42]. The differences in size particle distribution are related to the botanical sources and associated with the techno-functional properties of starches [39].

3.3. Pasting properties and gel texture

Fig. 2B shows a low pasting temperature (PT) (68.2 ± 0.2 °C), with a maximum increase in the CHS viscosity at peak viscosity (PV) of 666 ± 13 BU (Brabender units) (Table 2). The PV shows the capacity of CHS to hold water and the resistance of the swollen granules to rupture. The values of PV obtained in this work could be related to the particle size distribution, since low particle size distribution leads to a lower hydration capacity due to a limited filling space [43]. With regard to PV, CHS showed lower values than that reported for potatoes (1421 BU) but higher than wheat (333 BU) and corn starches (476 BU) [44]. As a consequence of the swelling, a rupture of the granule occurs, which generates a decrease in the viscosity of the paste; this phenomenon is known as breakdown (BD) and measures the stability of the pastes and the tendency of the granules to resist the shear force during the heating process [34]. The BD obtained for CHS was 290 ± 14 BU, reducing about 44 % of the maximum observed viscosity (PV). This decay value was similar to those observed in mung bean starch, for which a viscosity reduction of approximately 43 % was reported in the BD stage [39]. The setback (SB) and final viscosity (FV) of CHS were 220 ± BU, and 596 ± 6 BU, respectively. The SB and FV are related to the retrogradation tendency to amylose release from the BD stage starch granule, which has

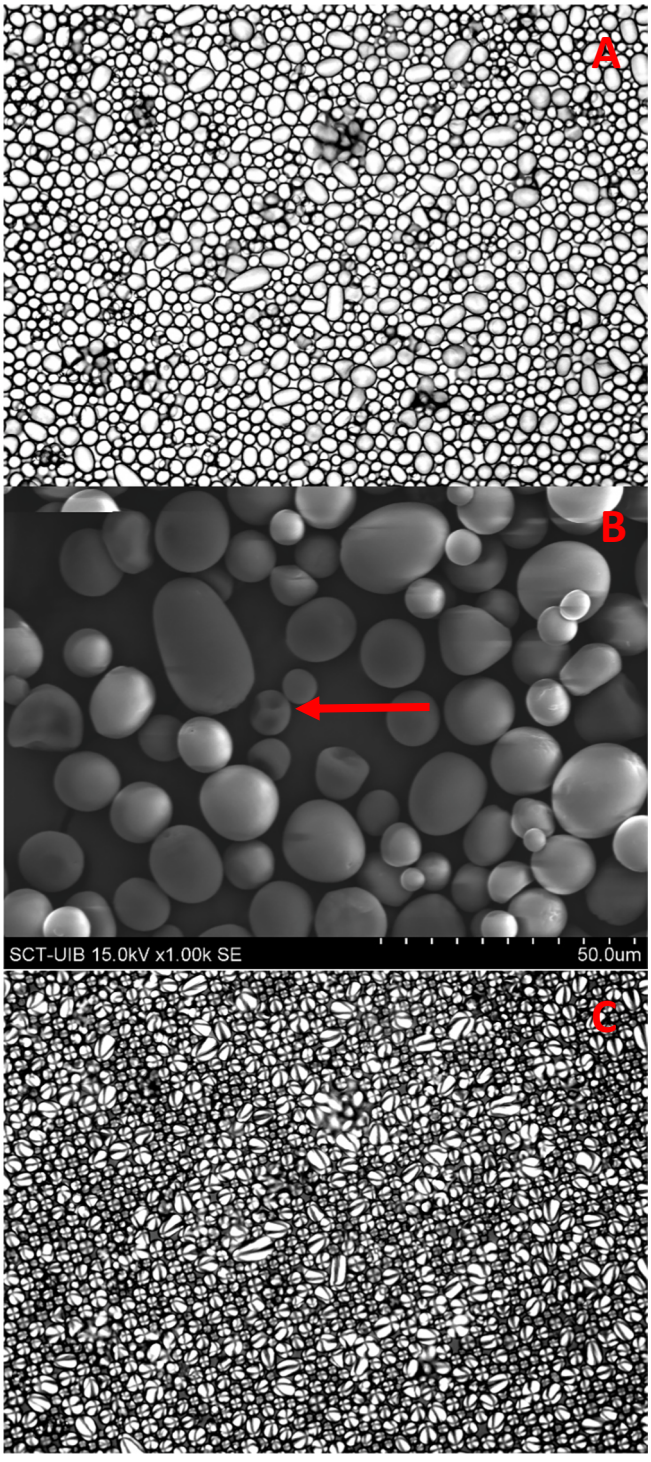

Fig. 1. Light microscope (A), scanning electronic microscope (B), and polarized light microscope (C) images of chachafruto starch.

strong reassociation capabilities [45]. The FV obtained for the analyzed starch was higher than for wheat starch [46].

The hardness, cohesiveness, and adhesiveness of the chachafruto starch gels were 49 ± 7 N, 0.07 ± 0.01 N, and 0.59 ± 0.05 N s^{-1}, respectively. The hardness of the chachafruto starch gel can be related to the starch's FV and apparent amylose content since high viscosity is partially associated with a molecular re-association in the BD process. In addition, amylopectin chain length can influence the hardness of the paste [33]. The hardness of the starch gel analyzed was higher than

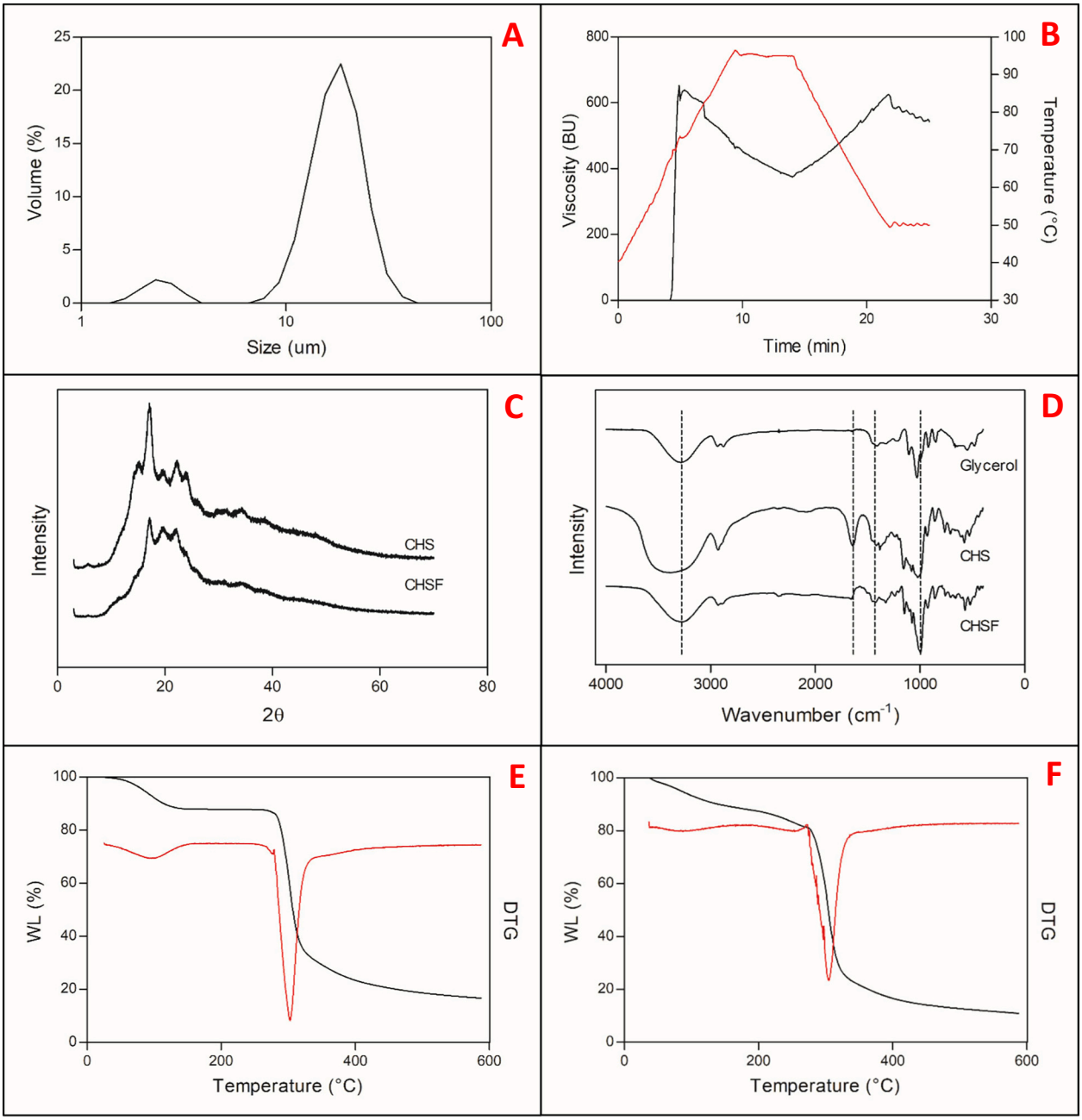

Fig. 2. (A) Particle size distribution, (B) pasting properties of chachafruto starch (CHS), (C) XRD diffractograms of CHS and film (with 2 % of CHS *w/v*), (D) FTIR spectrums of glycerol, CHS and film, (E) weight loss curve of CHS, (F) weight loss curve of film.

Table 2
Pasting properties of chachafruto starch.

Pasting properties	Value ± SD
Pasting temperature (PT, °C)	68.2 ± 0.2
Peak viscosity (PV, BU)	666 ± 13
Trough viscosity (TV, BU)	376 ± 2
Breakdown (BD, BU)	290 ± 14
Setback (SB, BU)	220 ± 4
Final viscosity (FV, BU)	596 ± 6

BU: Brabender Units. Values are expressed as means ± standard deviation of at least three repetitions.

values obtained for wheat starches [47]. Meanwhile, adhesiveness was higher than those reported for kidney bean starch, but the cohesiveness showed lower values than for the same species [40]. The results obtained in this work show a high capacity to form elastic pastes with the ability to retain their initial structure under mechanical stress.

3.4. X-ray diffraction (XRD) of starch

The X-ray diffraction of the starch is shown in Fig. 2C. The CHS exhibited a typical B-type pattern with peaks at 5.6, 15, 17, 20, 22, and 24° at diffraction angles of 2θ [23]. Although the C–type pattern is expected in starches extracted from legumes, different authors have reported the presence of a B–type pattern for starches obtained from various legumes such as wrinkled peas [48] and faba beans [49]. The X-ray diffraction pattern depends on the botanical origin and the organization of crystalline lamellae of amylopectin [41]. In addition, the starch showed relatively low crystallinity of 17.4 ± 1.1 %, which is in accordance with the crystallinity values reported for wrinkled peas (17.7 %)

[50], black bean (17.0 %), lentil (18.7 %), and chickpea (17.6 %) starches [48]. The relative crystallinity of the starch was low, which could be partly related to the intermediate apparent amylose content since it's amylopectin that mainly contributes to the crystalline structure in starch [41]. The crystallinity of starches also can be influenced by the length of the amylopectin chain, the orientation of the double helices, and the interaction between them [41].

3.5. Fourier-transform infrared (FTIR) spectroscopy

The Fourier-transform infrared (FTIR) spectrum of the native starch is shown in Fig. 2D. Native starch showed a broad band at 3400 cm^{-1} associated with the stretching of free hydroxyl groups [41]. The absorption peak exhibited at about 2900 cm^{-1} is related to the C—H bond stretching [35]. At the same time, the peak at 1650 cm^{-1} corresponds to the absorption of water molecules in the amorphous region of the starch [51]. Bands between 900 and 1100 cm^{-1} are sensitive to starch structure changes [32]. Thus, the bands observed at 970 cm^{-1} are associated with the bending vibration of C–O–H groups (water–starch interactions). Meanwhile, signals at 1025 cm^{-1} and 1080 cm^{-1} are related to the amorphous and crystalline structure of the starch [32]. Similar spectra have been reported for other starches obtained from legumes [35,41].

3.6. Thermal properties

The gelatinization temperatures [Onset (*To*), peak (*Tp*), and conclusion (*Tc*) temperatures] and the gelatinization enthalpy (ΔH) of the CHS are shown in Table 3. The *Tp* of CHS was similar to those reported for the same species and kidney bean [40], sorghum [36], and common bean (73–76 °C) starches [34]. However, this value was lower than those reported for starches obtained from young bamboo culm (78–80 °C) [38] and Talipot palm (82 °C) [52]. Compared with the same starches, the CHS showed an intermediate ΔH value. As Boudries [36] mentioned, low gelatinization temperature can indicate the low stability of starch crystallites in the granule and lower resistance to swelling. In addition, the ΔH is related to the energy required for the gelatinization process and the loss of molecular order for the dissociation of double helices [40]. These results are in accordance with the low degree of crystallinity of the CHS analyzed.

The thermogram of CHS is shown in Fig. 2E. For the analyzed starch, the degradation took place in three stages with a total weight loss of 83.7 ± 0.4 %. The first stage of degradation is related to water loss, which occurs in a temperature range between 55 °C to 134 °C with a maximum degradation peak at 93 °C and a weight loss of 12.1 ± 0.0 %, which is consistent with the moisture content of the sample. The second stage occurs in a temperature range of 278 °C and 321 °C (maximum degradation peak at 301 °C) with a loss of mass of 66.3 ± 0.2 %. This degradation is associated with the depolymerization of the carbonic chain [41]. The final stage occurs in temperatures above 330 °C and is associated with the formation of inert carbonaceous residues. The degradation of the analyzed starch agrees with the behavior reported for other starches [41,53].

Table 3
Thermal properties of chachafruto starch.

Pasting properties	Value ± SD
T_o (°C)	66.1 ± 0.6
T_p (°C)	71.1 ± 0.5
T_c (°C)	76.4 ± 0.9
ΔH (J g^{-1})	11.5 ± 1.0

T_o: onset temperature; T_p: peak temperature; *Tc*: conclusion temperature, ΔH: enthalpy of gelatinization. Values are expressed as means ± standard deviation of at least three repetitions.

3.7. Potential as food packaging of CHS

The chachafruto starch film (CHSF) exhibited peaks at 17, 20, and 22° at diffraction angles of 2θ, which indicates a partial loss of crystallinity due to the heating of the starch that generates the disruption of the granules (Fig. 2C). However, the reorganization of amylose and amylopectin chains in retrogradation provided a relative crystallinity value of 8.2 ± 0.4 %. The presence of an organized structure can positively impact the increasing barrier properties of the films, due to the increase in the organization of the structure, which will make the passage of water molecules more tortuous [23]. The crystallinity value observed for the film analyzed in this work is similar to that obtained for sweet potato starch films [11].

The CHSF and glycerol FTIR spectra are shown in Fig. 2D. Similar to native starch, CHSF presented bands at 3400 cm^{-1}, 2900 cm^{-1}, 1080 cm^{-1}, and 970 cm^{-1}. However, the signal at 1025 cm^{-1} in CHS had a slight shift towards 1018 cm^{-1} with an increase in peak intensity, which is related to an increase in the amorphous character of the film. In addition, a shift of the band corresponding to the stretching of the free hydroxyl groups towards a lower wavelength was observed, which can be associated with hydrogen interactions, as reported by Mantovan et al. [54]. The band at 3400 cm^{-1} also presented an intermediate intensity between that observed for glycerol and CHS, associated with the decrease in free hydroxyl groups by the interaction between glycerol and native starch and the reduction of the moisture content in the film analyzed. Similar observations have been made for films prepared with arracacha starch, glycerol, and PLA [55]. The CHSF results agree with those obtained in films prepared using non-conventional starches from different sources [23,56].

Regarding the thermal stability of the CHSF, the decomposition occurred in four stages with a total loss of mass of 89.1 ± 0.3 %. The first stage ranged from 55 °C to 128 °C related to the loss of water with a loss of mass of 10.8 ± 0.5 %. The second, ranging from 203 °C to 262 °C, is associated with the decomposition of glycerol used as a plasticizer (Fig. 2F) and exhibited a mass loss of 9.34 ± 1.01 %. The third stage occurred between 275 °C and 326 °C and showed the highest weight loss of the analyzed material (64.1 %), which is related to the depolymerization of carbonic chains. As in the degradation of pure starch, inert carbonaceous residue formation occurs at temperatures above 330 °C. Considering that the maximum degradation peak of the starch and the biodegradable film occurs at temperatures above 200 °C, it can be established that both materials exhibit high thermal stability [57].

The film obtained using CHS exhibited a continuous surface and cross-sectional without porosities, which could be related to the homogeneity of the material's interaction (Fig. 3). However, some roughness can be observed on the film surface, which can be attributed to the production method (casting method). The presence of continuous surfaces in the films has been reported as a desirable feature in the production of packaging materials as it helps to improve the barrier properties of the materials [58]. With regard to the properties of affinity for water, the CHSF showed values of swelling power (*SP*) and solubility (*S*) of 101 ± 1 % and 18.1 ± 0.9 %, respectively. The *S* is associated with the ability of films to resist degradation and loss of structure in an aqueous environment. CHSF *S* were lower than those observed in films prepared using chitosan mixed with cassava and potato starch [59] and similar to the values for ulluco starch [23]. The *SP* is the ability of a film to retain water in its structure, which can be improved by the presence of hydrophilic groups [26]. The *SP* was higher than that observed for films obtained from arracacha starch and Polylactic acid (PLA) [55] and similar to those reported for ulluco-based films [23].

The opacity of packaging materials is important in relation to their acceptability and the perception of the consumer. Thus, this parameter can define the final use of a material [55]. The CHSF showed an opacity value of 0.729 ± 0.08, demonstrating the high transparency of the material. The results obtained for the analyzed samples confirm that the films prepared with starch are highly transparent [12]; however, the

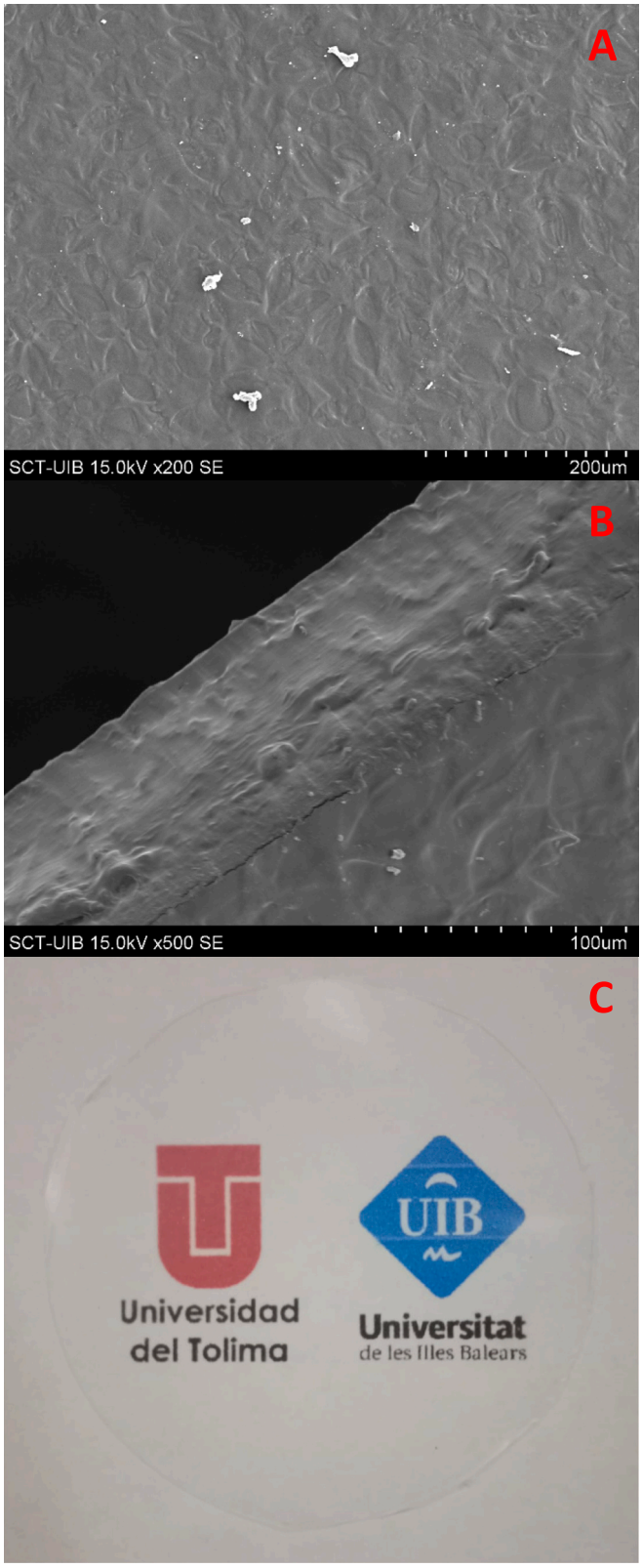

Fig. 3. SEM micrograph of surface (x 200) (A), cross-section (x 500) (B), and photographs (C) of chachafruto starch (CHS)-based film (prepared with 2 % of CHS w/v).

mixture of starch with another type of material, such as gums, proteins, and other polysaccharides, can reduce transparency [60].

The water vapor permeability (WVP) value of the CHSF was $2.3 \times 10^{-9} \pm 8.8 \times 10^{-11}$ g m^{-1} s^{-1} Pa^{-1}. This result is in accordance with those obtained for films prepared using cubio, pumpkin, lentil, and quinoa starches [1,13]. However, the WVP obtained was lower than those obtained using the same starch mixed with different concentrations of commercial oil [9]. The difference between the permeability of films obtained with starch extracted from the same species may be due to the amylose content, since a greater amount of amylose can help rearrange the chains after retrogradation and cause a consequent increase in the final crystallinity of the film [13]. The relationship between film crystallinity and permeability has been demonstrated in previous studies [1].

The CHSF showed elongation at break (EB), tensile strength (TS), and Young Modulus (YM) values of 40.1 ± 2.65 %, 3.68 ± 0.57 MPa, and 31.9 ± 3.4 MPa, respectively. The EB and TS results were higher than those reported for films prepared with starch of the same species and different commercial oil concentrations [9]. The differences observed may be due to the different concentrations of starch and plasticizer in the formulations, but mainly to the presence of higher amylose content in the starch analyzed in this work, which, as mentioned above, produces a greater ordering of the amylose/amylopectin chains after retrogradation. Additionally, the analyzed sample presented a higher EB than the potato, pumpkin, lentil, and quinoa starch films but a lower tensile strength [13].

3.8. Potential as food ink for 3D printing of CHS

3.8.1. Printability and morphology of 3D printing of CHS

The appearance and the microstructure of the 3D-printed pastes based on CHS are shown in Fig. 4. All concentrations of starch allowed good printability and produced stable structures. Despite this, it was observed that the lowest concentration of starch (3D printed at a CHS concentration of 8 %; CHS3D1) produced a structure with rounded corners but with well-defined and smooth lines. Meanwhile, increased starch concentration in the gels (3D printed at a CHS concentration of 10 %; CHS3D2, and 3D printed at a CHS concentration of 12 %; CHS3D3) produced a structure with regular corners but with irregularities on the four sides of the geometrical form (lines with some indentations). The ease of printability with the lower concentration gel paste can be associated with its lower viscosity, due to the lower concentration and, therefore, less interaction between amylose chains, amylopectin, and water molecules. Similar behavior was observed in 3D-printed oxidized maize starch at different concentrations (11 % to 19 % of starch) [20]. The authors reported that the best 3D prints were achieved at 11 % and 13 % starch concentrations; however, higher concentrations generated print defects possibly related to greater interaction between oxidized starch and water molecules. In addition, Liu et al. [21] showed that a low viscosity in potato starch gels improved printability but negatively affected the stability of 3D prints because the structure of the first layer was not strong enough to support subsequent layers and could collapse. The printability and degree of printing accuracy of the tested materials can affect consumer perception. In the food production process, low printing precision and sample collapse due to the low stability of the product can generate rejection by the consumer. Because of the low degree of gelatinization of CHS3D3, defects such as the structure collapse of the printed food could be caused by itself or in combination with other ingredients. On the other hand, CHS3D1 and CHS3D2 would present a greater resistance and printability.

With regard to the microstructure, it was observed that an increase in the starch concentration produced structures with a smaller pore size (higher cell density). In comparison, the lower concentration of CHS produced a larger pore size (lower cell density). Cells in the structure suggest that the gels and the 3D-printed geometries were formed under

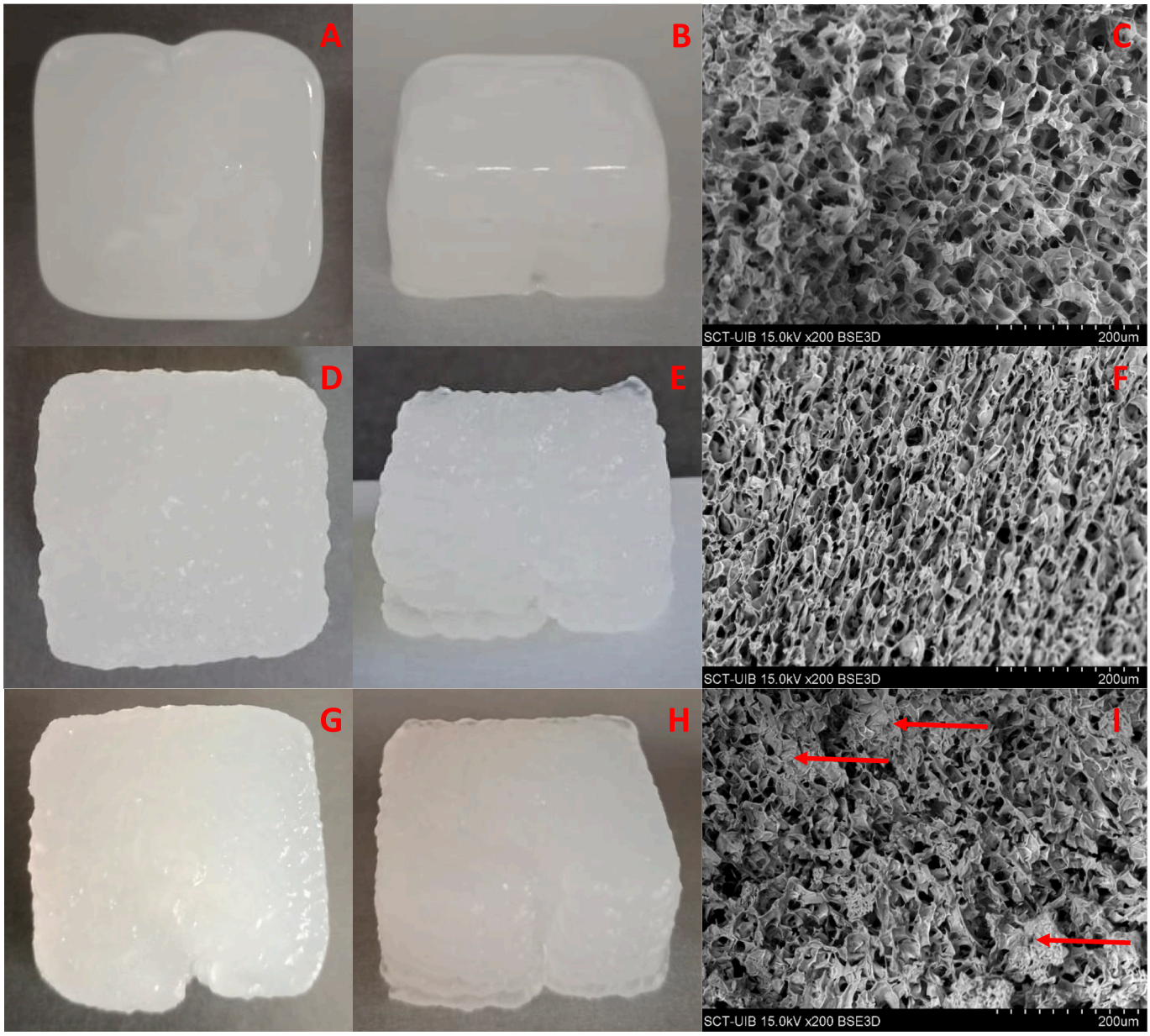

Fig. 4. Top, front view (photographs) and SEM micrographs of the structure of 3D prints based on chachafruto starch (CHS) prepared at different starch concentrations: 8 % (A-C), 10 % (D—F), and 12 % (G-I).

conditions that enabled CHS to gelatinize fully or partially and form a cross-linked network structure [29]. Despite the observation of network formation in sample CHS3D3, agglomeration of material could be observed due to the low degree of gelatinization, which may be because of the high concentration of starch and the short processing time (red arrows, Fig. 4F). The starch granules used for 3D printing undergo different degrees of gelatinization depending on their properties and the process parameters. These parameters include gelatinization time, gelatinization enthalpy, amylose content, and process temperature. Previous studies have demonstrated that the process temperature used for the gelatinization of corn starch affected the structure of the 3D prints [61]. At low temperatures (<70 °C and a gelatinization time of 15 min), the starch granules do not gelatinize sufficiently to form a cross-linked network structure. Meanwhile, high temperatures (>80 °C and a gelatinization time of 15 min) generated greater leaching of short chains in the retrogradation process, which have a lower capacity for interaction, leading to the formation of structures with microfractures. The formation of cross-linked network structures has also been described in 3D prints from potato and corn starches [20,29]. These structures were associated with 3D print properties such as water retention capacity and porosity. The authors found that lower starch concentrations produced more uniform network structures, enhancing water absorption. A higher starch concentration leads to denser networks related to the aggregation and entanglement of molecular chains. Although higher starch concentrations can form a more robust network, this also increases the fluid viscosity, hindering the sample flow through the nozzle and affecting printability. High starch concentrations, as in the case of CHS3D3, can generate this type of defect in the printed products.

3.8.2. *Crystallinity of 3D printing of CHS*

The 3D prints showed a crystallinity pattern similar to the CHS with signals at 5.6°,15°, 17, 20, 22, and 24° at diffraction angles of 2θ (Fig. 5). The crystallinity values of the samples were 3.4 %, 3.5 % and 5.6 % for CHS3D1, CHS3D2, and CHS3D3, respectively. The reduction of crystallinity compared with the native starch is due to the partial loss of the

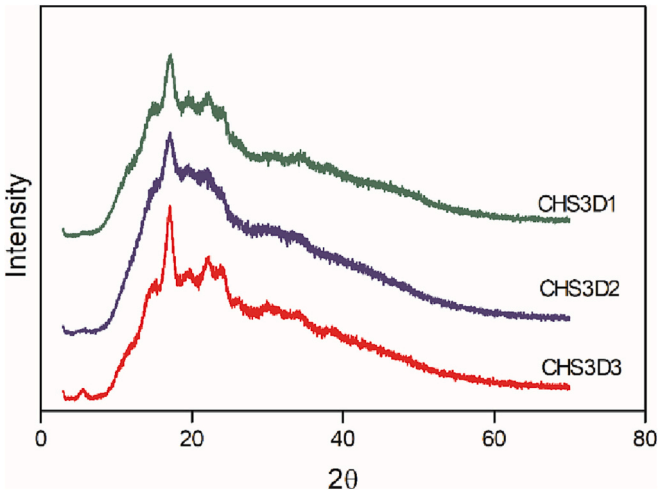

Fig. 5. XRD diffractograms of 3D prints based on chachafruto starch (CHS) prepared at different starch concentrations: 8 % (CHS3D1), 10 % (CHS3D2), and 12 % (CHS3D3).

organized structure because of a partial gelatinization of the starch. The differences between the crystallinity values of the prints may be because the temperature and time used in the preparation of the gels were insufficient for a total gelatinization of the starch. The decrease in the intensity of the peaks could be evidence of this. Similar observations were made for the crystallinity of 3D prints prepared with corn and potato starch [29,62]. In both cases, a decrease in crystallinity was observed after gelatinization and the printing of the gels. In the case of 3D prints prepared with corn starch, a gelatinization temperature of 90 °C was used for 25 min, achieving a partial decrease in crystallinity. However, the remaining crystallinity of the material prepared with the highest starch concentration, was associated with the re-crystallization of the starch chains during retrogradation. On the other hand, in the preparation of 3D prints obtained from potato starch, it was observed that both the starch concentration and the temperature affected the final value of crystallinity. Low starch concentrations (10 %) at an intermediate temperature (70 °C) led to the loss of the original crystalline structure. However, low treatment temperatures (<70 °C) with intermediate concentrations of starch (15 %) partially retained the original crystalline structure.

3.8.3. *Textural properties of the 3D printing of CHS*

Texture analysis can be related to sensory acceptability, as well as to the printability and overall stability of the product. Thus, a product that is poorly printed will exhibit poor textural properties. In addition, these textural properties are an essential sensory attribute of food acceptability [63]. The hardness of the samples analyzed was 2.1 ± 0.2 N (213 ± 23 g), 2.3 ± 0.4 N (231 ± 41 g), and 0.93 ± 0.02 N (95 ± 3 g) for CHS3D1, CHS3D2, and CHS3D3, respectively. Statistical differences were observed between CHS3D3 and samples CHS3D1 and CHS3D2 ($p < 0.05$). The low degree of hardness shown by the sample prepared with the highest starch content may be associated with the low degree of starch gelatinization, which limited the formation of the crosslinked network in the gel and subsequently in the 3D print. These results can be associated to the microstructure results where the deficient formation of the cells in the material is observed. The hardness values presented by samples CHS3D1 and CHS3D2 may be related to a greater starch gelatinization, leading to its retrogradation, and forming a more organized cross-linked network. Since the hardness of the samples is associated with the force necessary to deform them, it was observed that samples CHS3D1 and CHS3D2 showed an excellent ability to retain their initial shape after being subjected to a compressive force, in comparison with samples prepared from potato (105 g), wheat (167 g) and corn starches (105 g) [19,28,64]. According to Zheng et al. [28], starch syneresis and subsequent recrystallization of amylose and amylopectin were the main factors affecting the firmness of 3D prints from wheat starch.

Springiness is related to the elasticity of the samples and their ability to return to their original shape after being subjected to initial compression [18]. The values obtained for the samples analyzed were 0.92 ± 0.01, 0.91 ± 0.01, and 0.75 ± 0.01 for CHS3D1, CHS3D2, and CHS3D3, respectively ($p < 0.05$). Similar to the hardness values, the sample with the highest starch content (CHS3D3) presented the lowest values of springiness, which can be associated with the degree of gelatinization, leading in turn to low water retention. The samples obtained with CHS showed higher springiness values than those reported for samples printed from cassava, wheat, corn, sweet potato, potato, and buckwheat starches [17] and similar to those reported for native and annealing wheat starch [18].

Cohesiveness is a parameter related to the strength of the internal bonds of the sample and the degree to which they can be deformed before the break. Cohesiveness showed a similar trend to springiness and hardness, with values of 0.88 ± 0.10, 0.89 ± 0.07, 0.59 ± 0.02 for CHS3D1, CHS3D2, and CHS3D3, respectively ($p < 0.05$). As explained above, the partial gelatinization of starch in sample CHS3D3 generated a low release of amylose and amylopectin, affecting the network structure's generation and reducing the sample's cohesiveness. Samples CHS3D1 and CHS3D2 showed cohesiveness values comparable to those reported for 3D printing from potato, corn, and wheat starch [19] and annealing wheat starch [18]. This indicates a high consistency of the samples obtained with low and medium CHS concentrations.

3.8.4. *Dynamic mechanical analysis of the 3D printing of CHS*

The behavior of the storage modulus (G') and the loss modulus (G'') of the 3D samples is presented in Fig. 6. In all the samples, the value of G' increases as the frequency value increases. In contrast, the value of G'' tends to increase but then decreases. This behavior agrees with that reported for 3D gels printed using potato starch [15]. Additionally, it was observed that the value of G' was greater than G'' throughout the analysis, indicating that the samples presented a predominantly elastic character. This can be related to the ability of the material to maintain its shape [16]. Similar observations were made for gels used for 3D printing prepared from cassava, corn, wheat, potato, and buckwheat starches [17]. Among the samples evaluated, sample CHS3D1 presents the highest value of G', followed by sample CHS3D2 and sample CHS3D3. These results corroborate the observations made in the texture analysis for hardness. As previously mentioned, the sample with the highest starch content presented low gelatinization, negatively impacting the material's microstructure and, therefore, the dynamic-mechanical properties. On the other hand, the values of G' in the samples CHS3D1 and CHS3D2 can be related to a greater gelatinization and, therefore, a greater release of amylose [17]. However, the difference between these two samples may be due to cell structure and packing.

4. Conclusions

The native starch from chachafruto has a high extraction yield and low lipids, proteins, and ashes content. These characteristics indicate a high purity level and potential for consumer acceptance. The wet extraction method preserves the morphology of the starch granules without affecting their integrity. The technological properties of the material, such as texture and pasting properties, are influenced by its small particle size. The apparent amylose content of this starch was another factor that determined its physicochemical properties and industrial potential. The X-ray diffraction analysis revealed that the starch presents the typical characteristics obtained from legumes. Moreover, the thermal analysis indicated that the starch has excellent thermal stability, making it desirable for industrial use. Regarding the feasibility of producing food packaging, the chachafruto starch exhibited good mechanical, thermal, and barrier characteristics. These properties and

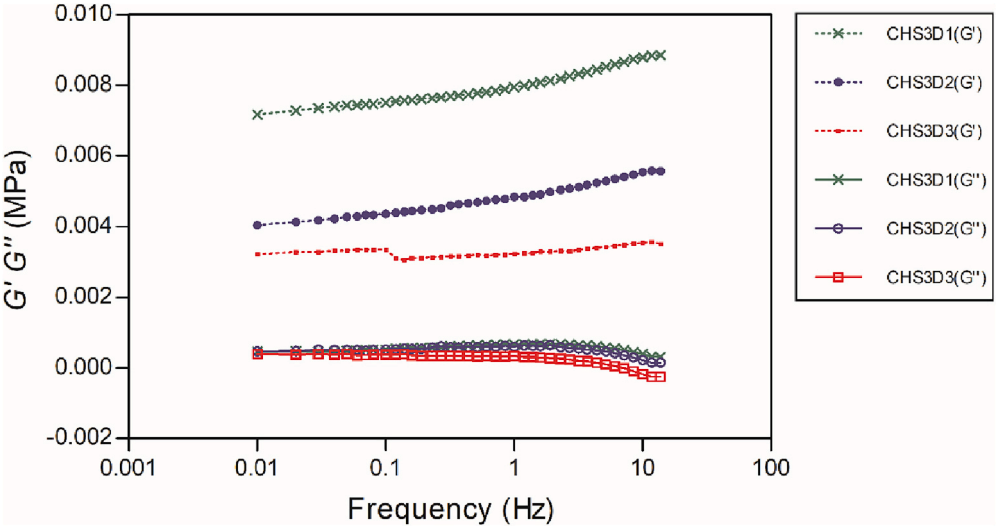

Fig. 6. Storage Modulus (*G'*) and Loss Modulus (*G''*) curves of 3D prints based on chachafruto starch (CHS) prepared at different starch concentrations: 8 % (CHS3D1), 10 % (CHS3D2), and 12 % (CHS3D3).

their affinity for water suggested that chachafruto starch-based films could suit food matrices with intermediate moisture contents. In addition, the high transparency of the starch-based films made them a potential material for products that are not very susceptible to oxidation and for products that require visualization by the consumer. Starch concentration affected the physical properties of the 3D prints under the process parameters used in this study. Although low-quality 3D prints were produced at the highest starch concentration, at the other concentrations chachafruto starch was a suitable ingredient for 3D printing food, as it showed good printability, integrity, texture, and microstructure. Further research should focus on optimizing the printing process; exploring the interaction of chachafruto starch with other ingredients and its impact on film preparation and 3D printing; as well as a complementary characterization that could determine the molecular distribution and lamellar ordering of the amylose and amylopectin chains within the granule. Considering these findings, chachafruto emerged as an unconventional source of starch with tremendous industrial potential; this study demonstrated viable strategies for adding value to chachafruto crops.

CRediT authorship contribution statement

Luis Daniel Daza: Conceptualization, Formal analysis, Investigation, Methodology, Validation, Writing – original draft, Visualization. **Miguel Ángel Montealegre:** Formal analysis, Writing – original draft. **Cristina Reche:** Formal analysis, Writing – original draft. **Angélica Sandoval Aldana:** Conceptualization, Funding acquisition, Supervision, Writing – original draft. **Valeria Soledad Eim:** Conceptualization, Funding acquisition, Supervision, Writing – original draft, Project administration. **Henry Alexander Váquiro:** Conceptualization, Funding acquisition, Supervision, Writing – original draft, Project administration.

Declaration of competing interest

The authors declare that they have no known competing financial interests or personal relationships that could have appeared to influence the work reported in this paper.

Acknowledgments

The authors acknowledge financial support from l'Oficina de Cooperació al Desenvolupament I Solidaritat (OCDS) de la Universitat de les Illes Balears (UIB) (project OCDS-CUD2022/02) and the Agencia Estatal de Investigación MCIN/AEI/10.13039/501100011033 through the project (PID2019- 106148RR-C43). We would also like to thank Dr. Joan Cifre, Dr. José F. González Morey, and Dr. Ferran Hierro Riu from the "Serveis Cientificotecnics" of the UIB for their technical assistance. As well as the "Postcosecha y Control de Calidad" laboratory at the Universidad del Tolima (Colombia).

References

[1] L.D. Daza, M. Umaña, S. Simal, H.A. Váquiro, V.S. Eim, Non-conventional starch from cubio tuber (Tropaeolum tuberosum): physicochemical, structural, morphological, thermal characterization and the evaluation of its potential as a packaging material, Int. J. Biol. Macromol. 221 (2022) 954–964, https://doi.org/10.1016/j.ijbiomac.2022.09.092.
[2] O.F. Vilpoux, J.F. Santos Silveira Junior, Global production and use of starch, starchy crop, Morphol. Extr. Prop. Appl. (2023) 43–66, https://doi.org/10.1016/b978-0-323-90058-4.00014-1.
[3] G. Li, S. Wang, F. Zhu, Physicochemical properties of quinoa starch, Carbohydr. Polym. 137 (2016) 328–338, https://doi.org/10.1016/j.carbpol.2015.10.064.
[4] M. Kaur, S. Singh, Physicochemical, morphological, pasting, and rheological properties of tamarind (Tamarindus indica L.) kernel starch, Int. J. Food Prop. 19 (2016) 2432–2442, https://doi.org/10.1080/10942912.2015.1121495.
[5] T.T.M. Duyen, N.T.M. Huong, N.T.L. Phi, P. Van Hung, Physicochemical properties and in vitro digestibility of mung-bean starches varying amylose contents under citric acid and hydrothermal treatments, Int. J. Biol. Macromol. 164 (2020) 651–658, https://doi.org/10.1016/j.ijbiomac.2020.07.187.
[6] O.A. Bedoya, M. Caicedo, Y. Guerrero, Obtención de un extracto proteico a partir de harina de chachafruto, Rev Univ. Salud. 14 (2012) 161–167.
[7] J.L. Correa, J.E. Zapata, B. Hernández-Ledesma, Release of bioactive peptides from Erythrina edulis (Chachafruto) proteins under simulated gastrointestinal digestion, Nutrients. 14 (2022), https://doi.org/10.3390/nu14245256.
[8] V. Delgado-Soriano, P. Cortés-Avendaño, A. Guevara-Pérez, Carlos Vílchez-Perales, Revista de Investigaciones Altoandinas Características físico-químicas de las semillas de pajuro (Erythrina edulis Triana) y propiedades funcionales después de la extrusión Physicochemical characteristics of Pajuro seeds (Erythrina edulis Triana) and func, Rev. Investig. Altoandin. 22 (2020) 3–263.
[9] J.L.S. Sandoval, P.E.R. Fonseca, A.O.H. Arévalo, E.E.P. Sira, J. Ricci, D. Dufour, Development and characterization of edible films from Chachafruto (Erythrina edulis Triana) starch, Starch/Staerke 73 (2021) 1–10, https://doi.org/10.1002/star.202000269.
[10] A. Intiquilla, K. Jiménez-Aliaga, F. Guzmán, C.A. Alvarez, A.I. Zavaleta, V. Izaguirre, B. Hernández-Ledesma, Novel antioxidant peptides obtained by alcalase hydrolysis of Erythrina edulis (pajuro) protein, J. Sci. Food Agric. 99 (2019) 2420–2427, https://doi.org/10.1002/jsfa.9449.
[11] I. Choi, D. Shin, J.S. Lyu, J.S. Lee, H. Geon Song, M.N. Chung, J. Han, Physicochemical properties and solubility of sweet potato starch-based edible films, food Packag. Shelf, Life. 33 (2022), 100867, https://doi.org/10.1016/j.fpsl.2022.100867.
[12] R. Thakur, P. Pristijono, J.B. Golding, C.E. Stathopoulos, C. Scarlett, M. Bowyer, S. P. Singh, Q.V. Vuong, Effect of starch physiology, gelatinization, and retrogradation on the attributes of rice starch-ι-carrageenan film, Starch/Staerke 70 (2018), https://doi.org/10.1002/star.201700099.

[13] P. Pająk, I. Przetaczek-Rożnowska, L. Juszczak, Development and physicochemical, thermal and mechanical properties of edible fi lms based on pumpkin, lentil and quinoa starches, Int. J. Biol. Macromol. 138 (2019) 441–449, https://doi.org/10.1016/j.ijbiomac.2019.07.074.
[14] E. Basiak, A. Lenart, F. Debeaufort, Effect of starch type on the physico-chemical properties of edible films, Int. J. Biol. Macromol. 98 (2017) 348–356, https://doi.org/10.1016/j.ijbiomac.2017.01.122.
[15] Y. Cui, C. Li, Y. Guo, X. Liu, F. Zhu, Z. Liu, X. Liu, F. Yang, Rheological & 3D printing properties of potato starch composite gels, J. Food Eng. 313 (2022), 110756, https://doi.org/10.1016/j.jfoodeng.2021.110756.
[16] X. Zeng, T. Li, J. Zhu, L. Chen, B. Zheng, Printability improvement of rice starch gel via catechin and procyanidin in hot extrusion 3D printing, Food Hydrocoll. 121 (2021), 106997, https://doi.org/10.1016/j.foodhyd.2021.106997.
[17] S. Ji, T. Xu, Y. Li, H. Li, Y. Zhong, B. Lu, Effect of starch molecular structure on precision and texture properties of 3D printed products, Food Hydrocoll. 125 (2022), https://doi.org/10.1016/j.foodhyd.2021.107387.
[18] L. Zheng, Q. Zhang, X. Yu, X. Luo, H. Jiang, Effect of annealing and heat-moisture pretreatment on the quality of 3D-printed wheat starch gels, Innov. Food Sci. Emerg. Technol. 84 (2023), 103274, https://doi.org/10.1016/j.ifset.2023.103274.
[19] L. Zheng, Y. Yu, Z. Tong, Q. Zou, S. Han, H. Jiang, The characteristics of starch gels molded by 3D printing, J. Food Process. Preserv. 43 (2019) 1–11, https://doi.org/10.1111/jfpp.13993.
[20] Z. Qiu, B. Zheng, J. Xu, J. Chen, L. Chen, 3D-printing of oxidized starch-based hydrogels with superior hydration properties, Carbohydr. Polym. 292 (2022), 119686, https://doi.org/10.1016/j.carbpol.2022.119686.
[21] Z. Liu, M. Zhang, B. Bhandari, C. Yang, Impact of rheological properties of mashed potatoes on 3D printing, J. Food Eng. 220 (2018) 76–82, https://doi.org/10.1016/j.jfoodeng.2017.04.017.
[22] AOAC, Official Methods of Analysis, 16th ed, 1995 (Washington DC), https://www.aoac.org/ (Washington DC).
[23] A. Galindez, L.D. Daza, A. Homez-Jara, V.S. Eim, H.A. Váquiro, Characterization of ulluco starch and its potential for use in edible films prepared at low drying temperature, Carbohydr. Polym. 215 (2019) 143–150, https://doi.org/10.1016/j.carbpol.2019.03.074.
[24] L. Lin, D. Guo, L. Zhao, X. Zhang, J. Wang, F. Zhang, C. Wei, Comparative structure of starches from high-amylose maize inbred lines and their hybrids, Food Hydrocoll. 52 (2016) 19–28, https://doi.org/10.1016/j.foodhyd.2015.06.008.
[25] N. Paramakrishnan, S. Jha, K. Jayaram Kumar, Characterization and evaluation of smart starch from Kyllinga nemoralis, Int. J. Biol. Macromol. 72 (2015) 1020–1026, https://doi.org/10.1016/j.ijbiomac.2014.09.065.
[26] A. Homez-Jara, L.D. Daza, D.M. Aguirre, J.A. Muñoz, J.F. Solanilla, H.A. Váquiro, Characterization of chitosan edible films obtained with various polymer concentrations and drying temperatures, Int. J. Biol. Macromol. (2018), https://doi.org/10.1016/j.ijbiomac.2018.03.057.
[27] Natural Machines, Advanced user settings explained, Knowl. Base. (2023). https://support.naturalmachines.com/portal/en/kb/articles/advanced-settings-explained.
[28] L. Zheng, J. Liu, R. Liu, Y. Xing, H. Jiang, 3D printing performance of gels from wheat starch, flour and whole meal, Food Chem. 356 (2021), 129546, https://doi.org/10.1016/j.foodchem.2021.129546.
[29] Z. Liu, H. Chen, B. Zheng, F. Xie, L. Chen, Understanding the structure and rheological properties of potato starch induced by hot-extrusion 3D printing, Food Hydrocoll. 105 (2020), 105812, https://doi.org/10.1016/j.foodhyd.2020.105812.
[30] Z. Yang, X. Chen, Z. Xu, N. Ji, L. Xiong, Q. Sun, Anti-freezing starch hydrogels with superior mechanical properties and water retention ability for 3D printing, Int. J. Biol. Macromol. 190 (2021) 382–389, https://doi.org/10.1016/j.ijbiomac.2021.08.235.
[31] E. Álzate Carvajal, V.D. Quintero Castaño, J.C. Lucas Aguirre, Determinación de las propiedades térmicas y composicionales de la harina y almidón de chachafruto (erytina edulis triana ex micheli), Temas Agrar. 18 (2013) 21–35, https://doi.org/10.21897/rta.v18i2.714.
[32] P. Martínez, F. Peña, L.A. Bello-Pérez, C. Núñez-Santiago, H. Yee-Madeira, C. Velezmoro, Physicochemical, functional and morphological characterization of starches isolated from three native potatoes of the Andean region, Food Chem. X. 2 (2019), 100030, https://doi.org/10.1016/j.fochx.2019.100030.
[33] L. Zhang, G. Li, S. Wang, W. Yao, F. Zhu, Physicochemical properties of maca starch, Food Chem. 218 (2017) 56–63, https://doi.org/10.1016/j.foodchem.2016.08.123.
[34] N.L. Vanier, J.P. de Oliveira, G.P. Bruni, S.L.M. El Halal, F.A. Villanova, E. Da R. Zavareze, A.R.G. Dias, P.Z. Bassinello, Characteristics of starch from different bean genotypes and its effect on biodegradable films, J. Sci. Food Agric. 99 (2019) 1207–1214, https://doi.org/10.1002/jsfa.9292.
[35] R. Kumar, G. Ghoshal, M. Goyal, Moth bean starch (Vigna aconitifolia): isolation, characterization, and development of edible/biodegradable films, J. Food Sci. Technol. 56 (2019) 4891–4900, https://doi.org/10.1007/s13197-019-03959-4.
[36] N. Boudries, N. Belhaneche, B. Nadjemi, C. Deroanne, M. Mathlouthi, B. Roger, M. Sindic, Physicochemical and functional properties of starches from sorghum cultivated in the Sahara of Algeria, Carbohydr. Polym. 78 (2009) 475–480, https://doi.org/10.1016/j.carbpol.2009.05.010.
[37] S. Punia, S.B. Dhull, K.S. Sandhu, M. Kaur, S.S. Purewal, Kidney bean (Phaseolus vulgaris) starch: a review, Legum. Sci. 2 (2020) 1–7, https://doi.org/10.1002/leg3.52.
[38] M.H.F. Felisberto, A.L. Beraldo, M.S. Costa, F.V. Boas, C.M.L. Franco, M.T.P. S. Clerici, Characterization of young bamboo culm starch from Dendrocalamus asper, Food Res. Int. 124 (2019) 222–229, https://doi.org/10.1016/j.foodres.2018.03.074.
[39] A. Kaur, K. Shevkani, N. Singh, P. Sharma, S. Kaur, Effect of guar gum and xanthan gum on pasting and noodle-making properties of potato, corn and mung bean starches, J. Food Sci. Technol. 52 (2015) 8113–8121, https://doi.org/10.1007/s13197-015-1954-5.
[40] R. Bajaj, N. Singh, A. Kaur, N. Inouchi, Structural, morphological, functional and digestibility properties of starches from cereals, tubers and legumes: a comparative study, J. Food Sci. Technol. 55 (2018) 3799–3808, https://doi.org/10.1007/s13197-018-3342-4.
[41] J. Li, S. Zhang, Z. Zhang, S. Ren, D. Wang, X. Wang, X. Wang, C. Zhang, M. Wang, Extraction and characterization of starch from yard-long bean (Vigna unguiculata (L.) Walp. ssp. unguiculata cv.-gr. sesquipedalis), Int. J. Biol. Macromol. 181 (2021) 1023–1029, https://doi.org/10.1016/j.ijbiomac.2021.04.127.
[42] I.M. Demiate, A.M. Figueroa, M.E.B. Zortéa Guidolin, T.P. Rodrigues dos Santos, H. Yangcheng, F. Chang, J. Lin Jane, Physicochemical characterization of starches from dry beans cultivated in Brazil, Food Hydrocoll. 61 (2016) 812–820, https://doi.org/10.1016/j.foodhyd.2016.07.014.
[43] M. Kazir, D. Gurevich, A. Groobman, M. Prabhu, Á. Israel, A. Golberg, Y.D. Livney, Physicochemical, rheological and digestibility characterization of starch extracted from the marine green macroalga Ulva ohnoi, Food Hydrocoll. 120 (2021), https://doi.org/10.1016/j.foodhyd.2021.106892.
[44] K. Almonaityte, G. Cizauskaite, J. Bendoraitiene, L. Peciulyte, R. Rutkaite, Peculiarities of cross-linking degree determination for the starches of different botanical origin, Starch/Staerke 73 (2021) 1–10, https://doi.org/10.1002/star.202100041.
[45] D.O. Parra, L.D. Daza Ramírez, A. Sandoval-Aldana, V.S. Eim, H.A. Váquiro, Annealing treatment of ulluco starch: effect of moisture content and time on the physicochemical properties, J. Food Process. Preserv. (2022) 1–11, https://doi.org/10.1111/jfpp.16353.
[46] W. Wang, Y.C. Shi, Gelatinization, pasting and retrogradation properties of hydroxypropylated normal wheat, waxy wheat, and waxy maize starches, Food Hydrocoll. 106 (2020), 105910, https://doi.org/10.1016/j.foodhyd.2020.105910.
[47] C.S. Gaines, M.Ö. Raeker, M. Tilley, P.L. Finney, J.D. Wilson, D.B. Bechtel, R. J. Martin, P.A. Seib, G.L. Lookhart, T. Donelson, Associations of starch gel hardness, granule size, waxy allelic expression, thermal pasting, milling quality, and kernel texture of 12 soft wheat cultivars, Cereal Chem. 77 (2000) 163–168, https://doi.org/10.1094/CCHEM.2000.77.2.163.
[48] R. Hoover, T. Hughes, H.J. Chung, Q. Liu, Composition, molecular structure, properties, and modification of pulse starches: a review, Food Res. Int. 43 (2010) 399–413, https://doi.org/10.1016/j.foodres.2009.09.001.
[49] S. Punia, S.B. Dhull, K.S. Sandhu, M. Kaur, Faba bean (Vicia faba) starch: structure, properties, and in vitro digestibility—a review, Legum. Sci. 1 (2019) 3–7, https://doi.org/10.1002/leg3.18.
[50] Y. Zhou, R. Hoover, Q. Liu, Relationship between α-amylase degradation and the structure and physicochemical properties of legume starches, Carbohydr. Polym. 57 (2004) 299–317, https://doi.org/10.1016/j.carbpol.2004.05.010.
[51] I. Dankar, A. Haddarah, F.E.L. Omar, M. Pujolà, F. Sepulcre, Characterization of food additive-potato starch complexes by FTIR and X-ray diffraction, Food Chem. 260 (2018) 7–12, https://doi.org/10.1016/j.foodchem.2018.03.138.
[52] M. Navaf, K.V. Sunooj, B. Aaliya, C. Sudheesh, J. George, Physico-chemical, functional, morphological, thermal properties and digestibility of Talipot palm (Corypha umbraculifera L.) flour and starch grown in Malabar region of South India, J. Food Meas. Charact. 14 (2020) 1601–1613, https://doi.org/10.1007/s11694-020-00408-1.
[53] M.E.E. Franklin, H.A. Pushpadass, B. Kumar, S. Kulkarni, M. Muthurayappa, R. Kandasamy, P. Venkatachalam, P. Vellingiri, Physicochemical, thermal, pasting and microstructural characterization of commercial Curcuma angustifolia starch, Food Hydrocoll. 67 (2017) 27–36, https://doi.org/10.1016/j.foodhyd.2016.12.025.
[54] J. Mantovan, G.T. Bersaneti, P.C.S. Faria-Tischer, M.A.P.C. Celligoi, S. Mali, Use of microbial Levan in edible films based on cassava starch, Food Packag. Shelf Life 18 (2018) 31–36, https://doi.org/10.1016/j.fpsl.2018.08.003.
[55] A.M. Sánchez Riaño, E.M. Alegría Vivas, H.P. Bermeo Andrade, Y. Bohórquez Pérez, H.S. Villada Castillo, L.D. Daza, C.P. Valenzuela Real, Physicochemical, structural, and thermal characterization of biodegradable film prepared using arracacha thermoplastic starch and polylactic acid, J. Food Meas. Charact. (2022), https://doi.org/10.1007/s11694-022-01491-2.
[56] F.G. Henning, V.C. Ito, I.M. Demiate, L.G. Lacerda, Food Science and Technology Graduate Program, State University of Ponta Grossa Department of Agri-food Industry, Food, and Nutrition (LAN), College of Agriculture, Carbohydr. Polym. Technol. Appl, 2021, 100157, https://doi.org/10.1016/j.carpta.2021.100157.
[57] M.S. Elmi Sharlina, W.A. Yaacob, A.M. Lazim, S. Fazry, S.J. Lim, S. Abdullah, A. Noordin, M. Kumaran, Physicochemical properties of starch from Dioscorea pyrifolia tubers, Food Chem. 220 (2017) 225–232, https://doi.org/10.1016/j.foodchem.2016.09.196.
[58] Y. Chen, L. Liao, H. Liu, Y. Wang, L. Zhang, L. Chen, L. Yu, Effect of annealing on morphologies and performances of hydroxypropyl methylcellulose/hydroxypropyl starch blends, J. Appl. Polym. Sci. 137 (2020) 1–8, https://doi.org/10.1002/app.49535.
[59] S. Santacruz, C. Rivadeneira, M. Castro, Edible films based on starch and chitosan. Effect of starch source andconcentration, plasticizer, surfactant's hydrophobic tail andmechanical treatment, Food Hydrocoll. 49 (2015) 89–94, https://doi.org/10.1016/j.foodhyd.2015.03.019.
[60] A. Nawab, F. Alam, M.A. Haq, Z. Lutfi, A. Hasnain, Mango kernel starch-gum composite films: physical, mechanical and barrier properties, Int. J. Biol. Macromol. 98 (2017) 869–876, https://doi.org/10.1016/j.ijbiomac.2017.02.054.

[61] B. Cheng, Yue, Kexin Liang, Yifan Chen, Wei Gao, Xuemin Kang, Tianze Li, Cui, Effect of molecular structure changes during starch gelatinization on its rheological and 3D printing properties, Food Hydrocoll. 137 (2023), 108364, https://doi.org/10.1016/j.foodhyd.2022.108364.
[62] S. Ahmadzadeh, A. Ubeyitogullari, Fabrication of porous spherical beads from corn starch by using a 3D food printing system, Foods 11 (2022), https://doi.org/10.3390/foods11070913.
[63] R. Theagarajan, J.A. Moses, C. Anandharamakrishnan, 3D extrusion printability of rice starch and optimization of process variables, Food Bioprocess Technol. 13 (2020) 1048–1062, https://doi.org/10.1007/s11947-020-02453-6.
[64] B.C. Maniglia, D.C. Lima, M. da Matta Júnior, A. Oge, P. Le-Bail, P.E.D. Augusto, A. Le-Bail, Dry heating treatment: a potential tool to improve the wheat starch properties for 3D food printing application, Food Res. Int. 137 (2020), https://doi.org/10.1016/j.foodres.2020.109731.